Journal of Alloys and Compounds 509 (2011) 5631–5636

Contents lists available at ScienceDirect

Journal of Alloys and Compounds

journal homepage: www.elsevier.com/locate/jallcom

MOCVD growth and characterizations of $B_xAl_{1-x}As$ and $B_xAl_{1-x-y}In_yAs$ alloys

Qi Wang[a,*], Xiaomin Ren[a], Lijuan Zhang[b], Yue Yang[a], Tianhe Li[a], Hui Huang[a], Yongqing Huang[a], Shiwei Cai[a]

[a] Key Laboratory of Information Photonics and Optical Communications (Beijing University of Posts and Telecommunications), Ministry of Education, Beijing 100876, People's Republic of China
[b] Beijing Polytechnic College, Beijing 100042, People's Republic of China

ARTICLE INFO

Article history:
Received 5 November 2010
Received in revised form 11 February 2011
Accepted 19 February 2011
Available online 24 February 2011

Keywords:
MOCVD
BAlAs
BAlInAs
AFM
Raman

ABSTRACT

Zinc-blende $B_xAl_{1-x}As$ and $B_xAl_{1-x-y}In_yAs$ alloys have been grown on exactly oriented (0 0 1)GaAs substrates by low pressure metalorganic chemical vapor deposition (LP-MOCVD). The influence of susceptor coating, growth temperature and gas-phase boron mole fraction on boron incorporation into AlAs has been comprehensively investigated. It has been found that boron incorporation into AlAs could be enhanced and the optimal growth temperature range of $B_xAl_{1-x}As$ alloys changed from 580 °C to 610 °C when SiC-coated graphite susceptors were replaced by the non-coated ones. In this study, the maximum boron composition x of 2.8% was achieved for the pseudomorphically strained $B_xAl_{1-x}As$ alloys. AFM measurements show that RMS roughness of $B_xAl_{1-x}As$ alloys increased sharply with the increase of gas-phase boron mole fraction. Raman spectra of $B_xAl_{1-x}As$ alloys show a linear increase of the BAs shift with boron composition x. Based on BAlAs deposition, bulk $B_xAl_{1-x-y}In_yAs$ (x = 1.9%) quaternary alloy was grown lattice-matched to GaAs successfully. Moreover, 10-period BAlAs/GaAs and BAlInAs/GaAs MQW heterostructures were also demonstrated.

1. Introduction

Recently, the incorporation of boron into conventional III–V binary and ternary compounds (e.g., GaAs, AlAs, GaP and InGaAs) has gained special attentions of many research groups to develop novel material systems for various potential applications. Up to now, several boron-incorporated alloys have been investigated experimentally. BGaAs ternary alloys with boron contents as high as several percents and lattice-matched BGaInAs quaternary alloys have been successfully grown on (0 0 1)GaAs substrates by MOCVD [1–6]. In addition, applications of BGa(In)As alloys for nano-/micro-tubes and high-efficiency multijunction solar cells have also been demonstrated [7–9]. Moreover, BGaP alloys grown on Si substrates by MOVPE allow for the strain compensation of the active Ga(NAsP) laser material on Si [10]. Unfortunately, very limited experimental studies on boron incorporation into AlAs are available [2,11–13]. Especially, there is no report of the synthesis of BAlInAs quaternary alloys and the growth mechanism and key properties of BAl(In)As alloys are still not well known. However, BAl(In)As material system can be potentially used as the lower refractive-index materials of high-reflectivity DBRs, optical waveguide materials and potential barriers of semiconductor lasers. In addition, BAl(In)As material systems can also be used for the application of strain engineering (e.g., strain compensation for MQWs and QDs) and GaAs-based monolithic optoelectronic integration, etc.

In this paper, we report the LP-MOCVD growth of zinc-blende $B_xAl_{1-x}As$ alloys with boron composition varying up to 2.8% and 10-period BAlAs/GaAs MQW structure on GaAs using triethylboron as boron precursor. Boron incorporation behavior, crystalline quality, surface morphology and Raman properties of bulk $B_xAl_{1-x}As$ alloys are investigated in detail. We also report the growth of lattice-matched $B_xAl_{1-x-y}In_yAs$ quaternary alloys with boron composition of 1.9% and the corresponding 10-period BAlInAs/GaAs MQW structure for the first time.

2. Experimental procedure

In this study, zinc-blende $B_xAl_{1-x}As$, $B_xAl_{1-x-y}In_yAs$ alloys and the corresponding MQW heterostructures had been grown on exactly-oriented (0 0 1)GaAs substrates by LP-MOCVD. All the growths were performed in a Thomas-Swan 3×2″ vertical reactor at the constant low pressure of 133 mbar (100 Torr). GaAs substrates were positioned in the recessed wafer pockets on a graphite susceptor with or without SiC coating, which was heated by three separate graphite radial heating zones. Triethylboron (TEB), trimethylaluminium (TMAl), trimethylgallium (TMGa), trimethylindium (TMIn) and pure arsine (AsH_3) were used as B, Al, Ga, In and As source, respectively. The vapor pressure of TEB is 18 Torr at 5 °C. Pd-cell purified hydrogen (H_2) served as the carrier gas and the total flow rate was 12 slm.

The boron composition was varied by changing the growth temperature (T_g) and gas-phase boron mole fraction (X_v). X_v is used to quantify the boron concentration in the group III gas phase, which is defined as follows:

$$\text{For } B_xAl_{1-x}As, \quad X_v = \frac{[TEB]}{[TEB] + [TMAl]} \tag{1}$$

* Corresponding author. Tel.: +86 10 62284004 88; fax: +86 10 62284004 88.
E-mail address: wangqi@bupt.edu.cn (Q. Wang).

0925-8388/$ – see front matter © 2011 Elsevier B.V. All rights reserved.
doi:10.1016/j.jallcom.2011.02.104

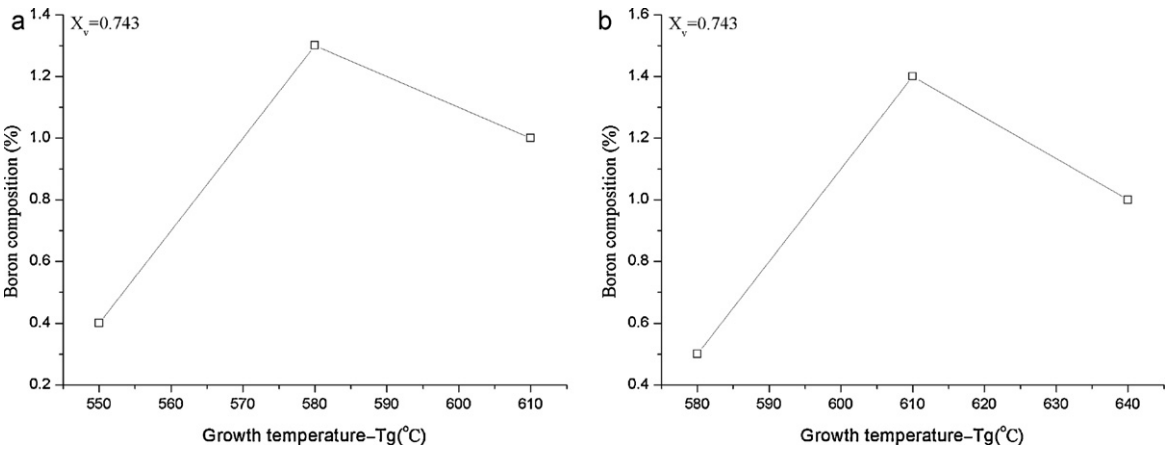

Fig. 1. Boron composition of $B_xAl_{1-x}As$ alloys measured by DCXRD as a function of T_g at $X_v = 0.743$(a) Graphite susceptor with SiC coating; (b) Graphite susceptor without SiC coating.

$$\text{For } B_xAl_{1-x-y}In_yAs, \quad X_v = \frac{[TEB]}{[TEB] + [TMIn] + [TMAl]} \tag{2}$$

where [TEB], [TMAl] and [TMIn] represented the input mole flow rate of TEB, TMAl and TMIn, respectively.

We grew two types of layered structures: (1) three-layered sandwich structures, which was composed of a 150-nm-thick GaAs buffer layer, a 100-nm-thick BAlAs or BAlInAs layer and a 25-nm-thick GaAs cap layer. For $B_xAl_{1-x}As$ growth, the mole flow rate of TEB was varied in the range of 3.06×10^{-5} to 8.16×10^{-5} mol/min. For $B_xAl_{1-x-y}In_yAs$ growth, the mole flow rate of TEB was set to 5.1×10^{-5} mol/min. In addition, the mole flow rate of TMAl, TMGa and AsH_3 were fixed to 1.4×10^{-5}, 1.4×10^{-5} and 2.7×10^{-3} mol/min for the corresponding layers from run to run, respectively, (2) 10-period multiple quantum-well (MQW) structures containing BAlAs or BAlInAs well separated by GaAs barrier. In our experiments, all the layers were grown at the same temperature.

A series of boron-incorporated samples with various boron compositions had been grown under the growth conditions described above. High resolution double crystal X-ray diffraction (DCXRD) ω-2θ scan using the symmetric (0 0 4) reflection was performed to determine the boron composition (x) by the separation angle between the diffraction peak of $B_xAl_{1-x}As$ alloys and that of GaAs substrate. The lattice constant of ternary $B_xAl_{1-x}As$ alloys can be expressed as $a_{BAlAs}(x) = 5.6611 - 0.8841x$. In this study, the BAlAs-related layered structures were pseudomorphically strained (i.e. no strain relaxation occurred). Assuming BAs Poisson ratio of 0.3, the boron composition (x) could be calculated from the DCXRD patterns. DCXRD measurement was also used to evaluate the lattice-mismatch ($\Delta a/a$) of $B_xAl_{1-x-y}In_yAs$ quaternary alloys and the crystalline quality of boron-incorporated alloys. Surface morphologies of BAlAs and BAlInAs alloys were observed by atomic force microscopy (AFM). Optical properties of BAlAs alloys were investigated by Raman spectroscopy. Depth profiles of the B, Al, Ga, In and As elements in the BAlInAs alloy were measured by secondary ion mass spectrometry (SIMS).

3. Results and discussion

3.1. BAlAs alloys

In our study, it has been found that boron incorporation strongly depends on the growth temperature (T_g) and gas-phase boron mole fraction (X_v). In addition, our experimental results indicate that susceptor coating influences the boron incorporation into AlAs. Fig. 1 shows the solid boron composition x as a function of the growth temperature T_g at $X_v = 0.743$. From Fig. 1a, it can be clearly observed that $x = 1.3\%$ was the highest boron composition, which demonstrated that $T_g = 580\,^\circ C$ should be the optimal temperature range for the LP-MOCVD growth of zinc-blende $B_xAl_{1-x}As$ alloys using SiC-coated graphite susceptor. When T_g was increased to 610 °C, the boron composition x dropped to 1.0%. Similarly, the boron composition x fell off sharply to 0.4% at the lower temperature of 550 °C. We think the growth mechanism of BAlAs and BGaAs alloys were very similar and the temperature dependence of boron incorporation into AlAs is also reaction kinetics determined like BGaAs alloys [5,13,14].

When the non-coated graphite susceptor was used for BAlAs growth, the boron incorporation efficiency was slightly enhanced, the highest boron composition increased to 1.4%. Meanwhile, the optimal temperature range increased to 610 °C (see Fig. 1b). This phenomenon had also been found in our growth of BGaAs alloys. In the experiment, we found that susceptor coating has an effect on the wafer surface temperature. When BAlAs growth using SiC-coated graphite susceptor at 580 °C was changed into that using non-coated susceptor at 610 °C, real wafer surface temperature increased nearly 20 °C. Obviously, higher surface temperature will promote the pyrolysis efficiency of TEB source. This might be the key cause for the enhanced boron incorporation.

Fig. 2 shows the solid boron composition x as a function of gas-phase boron mole fraction X_v for two types of susceptor at respective optimal growth temperature range. We found that solid boron composition (x) increased with X_v at the given growth temperature. For $B_xAl_{1-x}As$ alloys grown by the SiC-coated graphite susceptor at 580 °C, the splitting between (0 0 4) diffraction peak of $B_xAl_{1-x}As$ layers and that of GaAs substrate increased from +165 arcsec to +728 arcsec with the increment of X_v value from 0.743 to 0.853 (see Fig. 3). Accordingly, solid boron composition x increased from 1.3% to 2.7%. Boron composition x reached 1.4% at $X_v = 0.784$ (peak splitting is +200 arcsec) and 1.5% at $X_v = 0.813$ (peak splitting

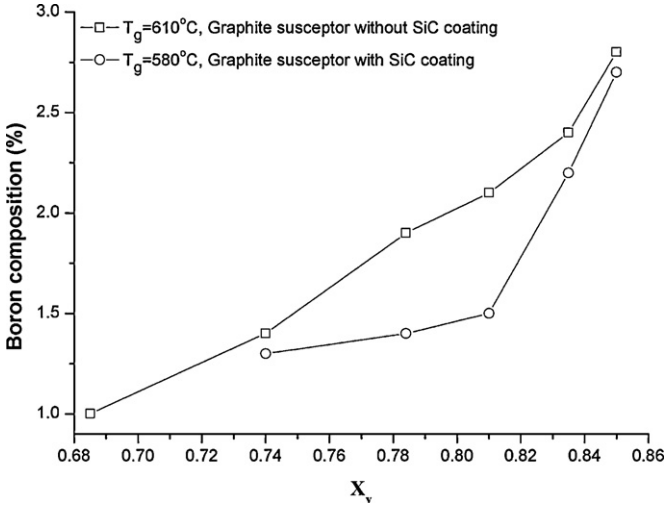

Fig. 2. Solid boron composition x determined by DCXRD as a function of X_v for $B_xAl_{1-x}As$ alloys grown on the graphite susceptor without SiC coating (solid lines with open squares) and with SiC coating (solid lines with open circles).

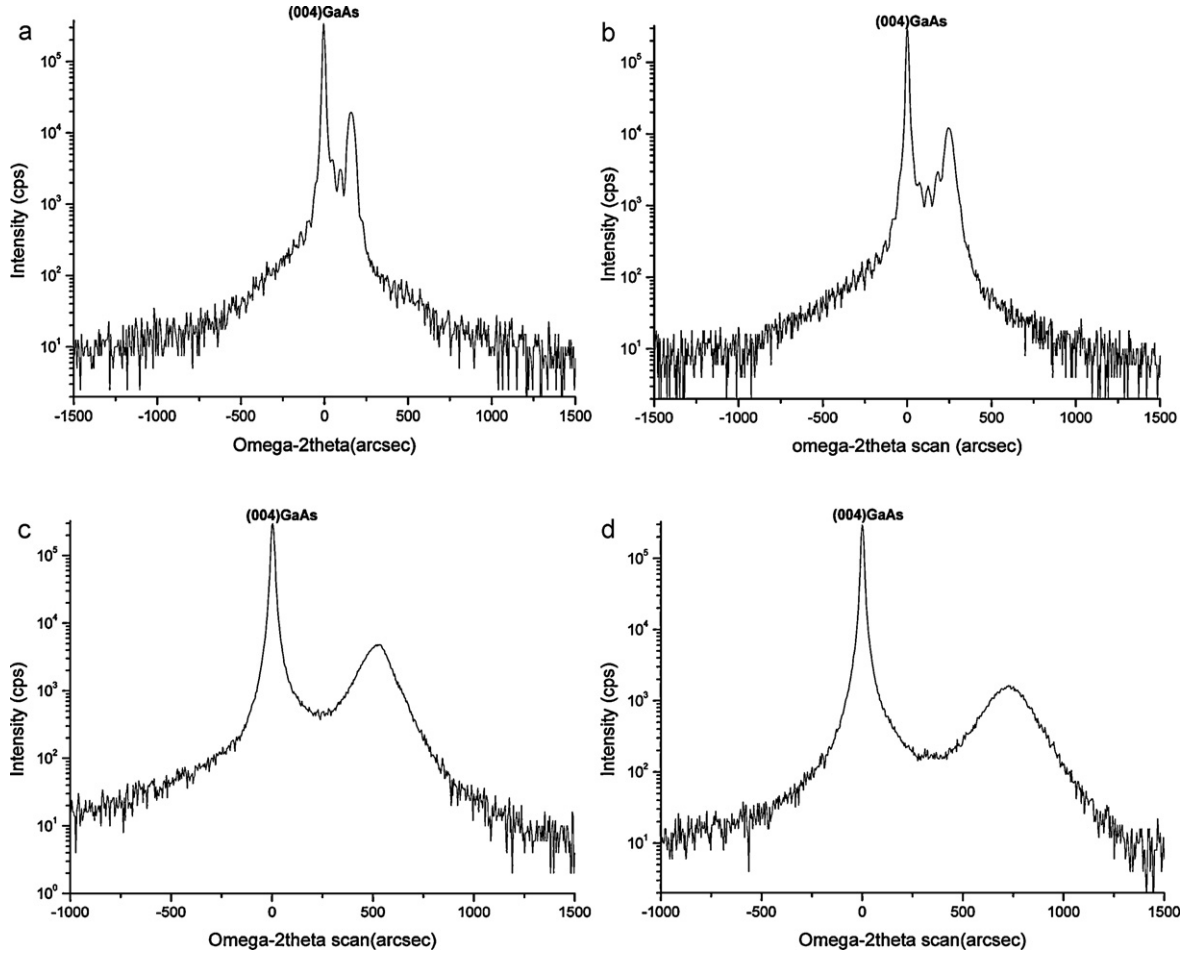

Fig. 3. DCXRD ω-2θ scan patterns of $B_xAl_{1-x}As$ samples grown on SiC-coated susceptor at 580 °C with X_v = (a) 0.743; (b) 0.813; (c) 0.835; and (d) 0.853.

is +244 arcsec), and the maximum boron composition of 2.7% was achieved at X_v = 0.853. As shown in our previous work, boron composition x of $B_xGa_{1-x}As$ alloys grown by the SiC-coated susceptor at 580 °C reached 5.8% at X_v = 0.813 [2]. Therefore, the incorporation efficiency of boron into AlAs was a little lower than that into GaAs under the same growth conditions. But in Ref. [11], it has been found that the incorporation efficiency of boron into GaAs is smaller than that into AlAs under the same X_v value at 550 °C, which is inconsistent with our experimental results. We estimate such a different behavior is likely to be caused by the different reactor pressure (133 mbar in this study and 50 mbar in Ref. [11]) and different growth temperature (580 °C, 610 °C in this study and 550 °C in Ref. [11]) employed. For BAlAs growth using TEB and TMAl with AsH_3 at relatively higher growth temperature and higher reactor pressure, there may exist parasitic reactions due to highly reactive feature of TMAl, which causes the significant reduction of boron incorporation efficiency.

For $B_xAl_{1-x}As$ alloys grown by the non-coated graphite susceptor at 610 °C, the splitting between (0 0 4) diffraction peak of $B_xAl_{1-x}As$ layers and that of GaAs substrate increased from +52 arcsec to +788 arcsec with the increment of X_v value from 0.685 to 0.853 (not shown here). Accordingly, solid boron composition x increased from 1.0% to 2.8%. Boron composition x reached 1.9% X_v = 0.784 (peak splitting is +408 arcsec) and 2.1% at X_v = 0.813 (peak splitting is +500 arcsec), and the maximum boron composition of 2.8% was achieved at X_v = 0.853, which also demonstrated the enhancement of boron incorporation.

Single-crystalline, zinc-blende $B_xAl_{1-x}As$ alloys with mirror-like surfaces and sharp diffraction peaks were obtained with the X_v value up to 0.813 for both types of susceptor. Further increase of X_v value (X_v > 0.813) resulted in the breakdown of crystal structure and the deterioration of surface morphology, which was indicated by the visible dark gray and hazy surfaces. Furthermore, along with the increase of X_v value, the full-width at half-maximum (FWHM) value of (0 0 4)BAlAs diffraction peak increased (e.g., for SiC-coated susceptor, the FWHM value increased from +44 arcsec to +204 arcsec with the increment of X_v value from 0.743 to 0.853), and the intensity of BAlAs diffraction peak decreased simultaneously (see Fig. 3), both of which also demonstrated the gradual degradation of the crystalline quality of $B_xAl_{1-x}As$ alloys.

Surface morphology of the $B_xAl_{1-x}As$ samples grown on non-coated susceptor at 610 °C was observed by NanoScope III AFM system. AFM images taken over the scanned area of 10 μm × 10 μm were presented in Fig. 4, which showed the evolution of surface morphology with the increase of X_v value clearly. From the measurement results, it could be found that RMS roughness would sharply increase as X_v value was increased. Measured root mean square (RMS) roughness of the mirror-like $B_xAl_{1-x}As$ samples grown with X_v = 0.784 and X_v = 0.813 were 11.3 nm and 17.8 nm, respectively, which were much larger that that of mirror-like $B_xGa_{1-x}As$ samples we grown in Ref. [1]. Both X_v = 0.835 and X_v = 0.853 yielded the hazy and rough surface, RMS roughness jumped to 25.3 nm and 34.0 nm suddenly, which indicated the obvious deviation from single crystal growth driven by the large miscibility gap (phase separation) between BAs and AlAs (as seen in Fig. 4c and d).

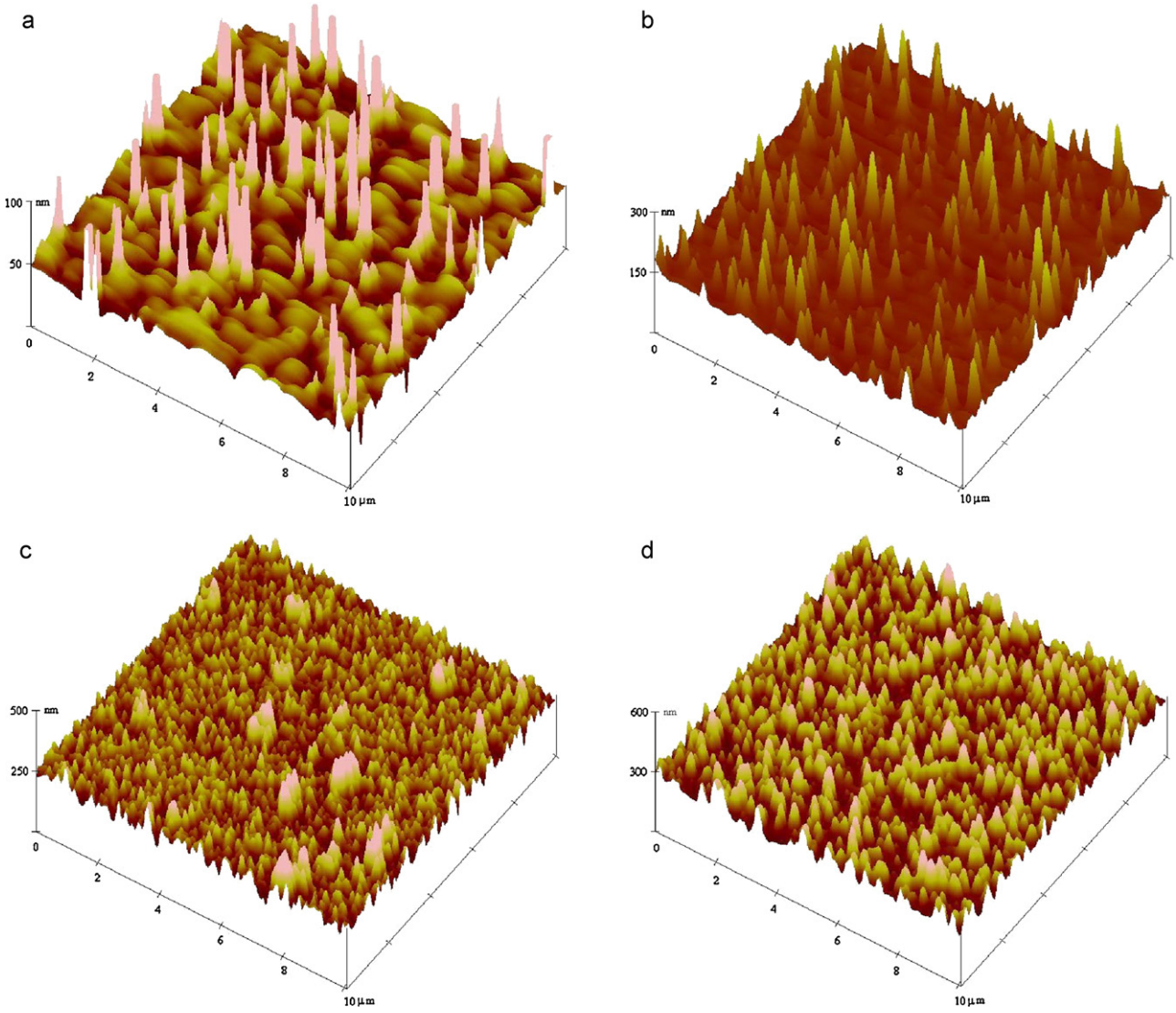

Fig. 4. AFM images of $B_xAl_{1-x}As$ samples grown on non-coated susceptor at 610 °C with X_v = (a) 0.784; (b) 0.813; (c) 0.835; and (d) 0.853.

In this study, room-temperature Raman spectroscopy was used to investigate the optical properties of $B_xAl_{1-x}As/GaAs$ alloys for the first time. Fig. 5 shows the Raman scattered spectra of $B_xAl_{1-x}As/GaAs$ alloys with three different boron composition *x*. Two vibrational peaks ranging from 260 cm^{-1} to 300 cm^{-1} are attributed to TO and LO phonons of GaAs, other two peaks ranging from 350 cm^{-1} to 400 cm^{-1} are attributed to TO and LO phonons of AlAs sub-lattice of $B_xAl_{1-x}As$ alloys (AlAs-like). And, we note that the TO phonons of GaAs and AlAs are highly suppressed in this Raman scattering configuration. In addition, two phonon peaks in the range of 510–540 cm^{-1} could also be clearly observed in each spectrum, which were due to LO phonons of BAs sub-lattice of $B_xAl_{1-x}As$ alloys (BAs-like). As we know, boron (B) element has two stable isotopes of ^{11}B (80.2%) and ^{10}B (19.8%) in the nature. Therefore, one of these two BAs-like vibrational peaks is for ^{11}BAs (lower energy side) and the other is for ^{10}BAs (higher energy side) [15]. We found the Raman shifts of BAs-like LO phonons were sensitive to the boron composition *x*. The peak position of BAs LO phonons shifted to the higher energy side as the boron composition *x* increased from 1.4% to 2.1%, and thereinto, LO (^{11}BAs) peak shifted from 511.23 cm^{-1} to 514.54 cm^{-1}, LO (^{10}BAs) peak shifted from 533.18 cm^{-1} to 536.48 cm^{-1}. Moreover, the Raman shifts of BAs-like LO phonons are nearly linear with the boron composition *x*.

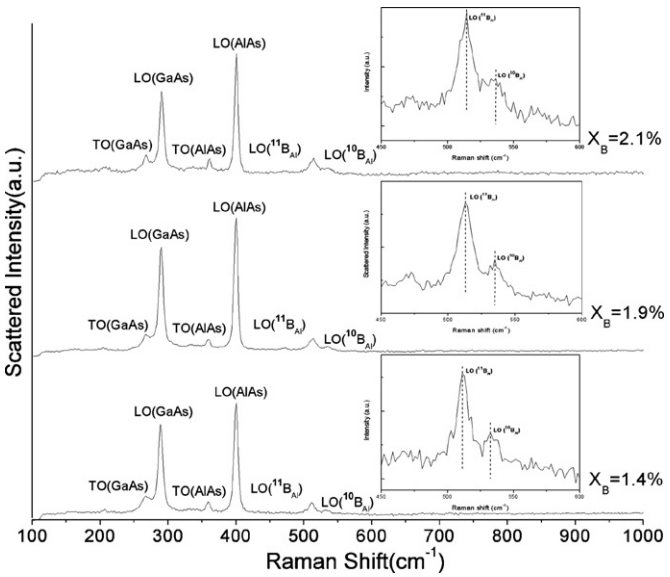

Fig. 5. Raman spectra of $B_xAl_{1-x}As$ alloys with boron composition of 1.4%, 1.9% and 2.1%, respectively. The inserts are Raman spectra of $B_xAl_{1-x}As$ alloys in the vicinity of the BAs-like LO phonon peaks.

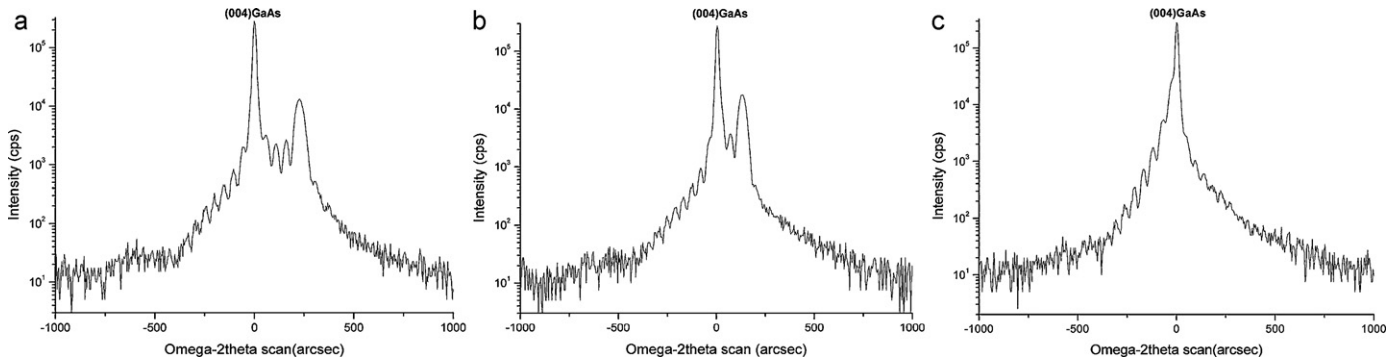

Fig. 6. DCXRD ω-2θ scan pattern of the $B_xAl_{1-x-y}In_yAs$ samples grown at 610 °C with X_v = (a) 0.774; (b) 0.768; and (c) 0.762.

3.2. BAlInAs alloys

Quaternary $B_xAl_{1-x-y}In_yAs$ alloys had also been deposited on (0 0 1)GaAs substrates by simultaneously feeding a small amount of TMIn source into the reactor during the growth of $B_xAl_{1-x}As$. BAlInAs growth was also performed by non-coated graphite susceptor at T_g = 610 °C. As mentioned above, the mole flow rate of TEB, TMAl and AsH_3 was still kept as 5.1×10^{-5}, 1.4×10^{-5} and 2.7×10^{-3} mol/min, respectively. The mole flow rate of TMIn increased from 6.43×10^{-7} mol/min to 2.14×10^{-6} mol/min, which caused X_v value to be varied in a very small range of 0.759–0.776.

Because the contraction of lattice constant caused by the addition of boron into AlAs can be offset by the further introduction of indium, in this experiment, with the increment of the mole flow rate of TMIn, the separation angle between (0 0 4) diffraction peak of $B_xAl_{1-x-y}In_yAs$ epilayer and that of GaAs substrate decreased from +408 arcsec to −64 arcsec. Obviously, high flexibility in the strain compensation can be offered by these BAlInAs quaternary alloys. DCXRD (0 0 4) diffraction patterns of three $B_xAl_{1-x-y}In_yAs$ samples are shown in Fig. 6. Both distinct Pendellösung fringes and sharp diffraction peak of BAlInAs that imply the good crystallinity of quaternary BAlInAs alloys could be clearly observed from the DCXRD patterns (see Fig. 6a and b). We noticed that $B_xAl_{1-x-y}In_yAs$ became lattice-matched to GaAs substrate at X_v = 0.762, i.e. [TMIn] = 1.82×10^{-6} mol/min (see Fig. 6c). In this study, we assumed that boron composition of $B_xAl_{1-x-y}In_yAs$ kept unchanged compared with that of $B_xAl_{1-x}As$ grown under the identical growth conditions. Additionally, $B_xAl_{1-x-y}In_yAs$ will be lattice-matched to GaAs under the condition of $y = 2.226x - 0.0196$ assuming Vegard's law. Thus, boron and indium composition of this lattice-matched $B_xAl_{1-x-y}In_yAs$ alloy can be regarded as 1.9% and 4.2%, respectively.

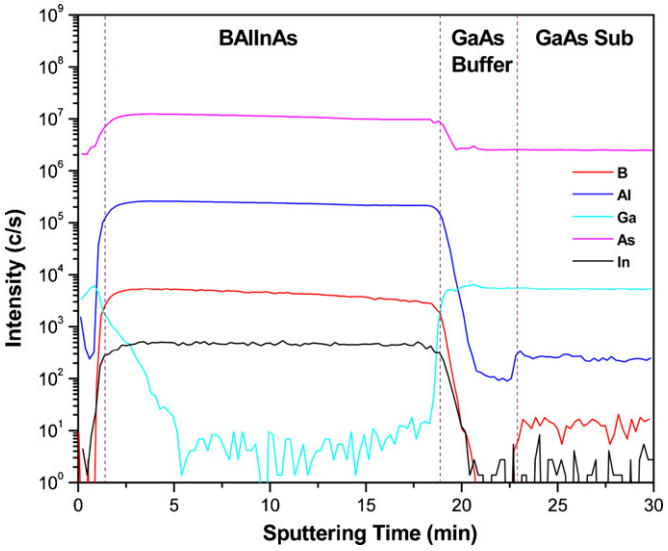

Fig. 7. SIMS depth profiles of the elements in lattice-matched $B_xAl_{1-x-y}In_yAs$ (x = 1.9%) sample grown at 610 °C.

RMS roughness of this lattice-matched BAlInAs sample over 10 μm × 10 μm was 10.0 nm (AFM image not shown), which was smaller than that of the corresponding $B_xAl_{1-x}As$ alloy (x = 1.9%). Depth profiles of B, Al, Ga, In and As element in lattice-matched $B_xAl_{1-x-y}In_yAs$ alloy with boron composition x of 1.9% are shown in Fig. 7. SIMS measurements showed that the boron distribution in

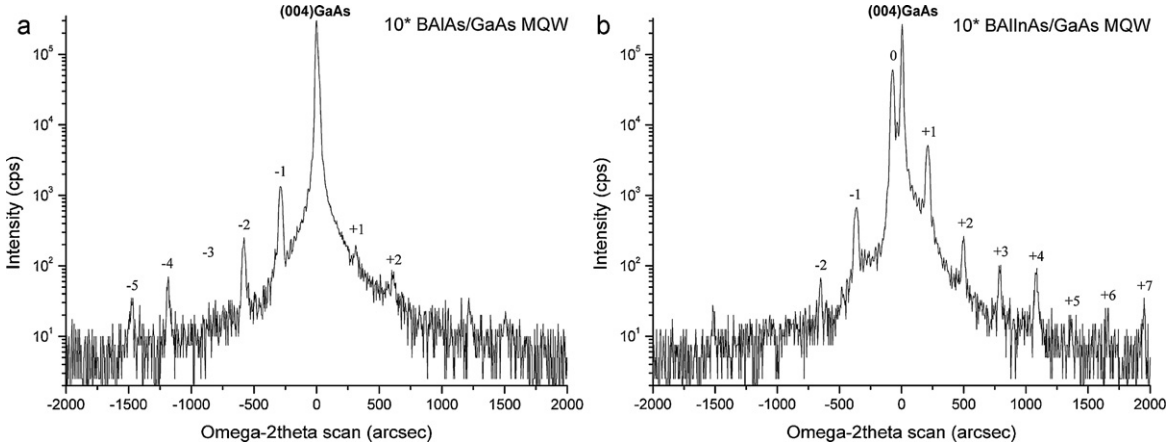

Fig. 8. DCXRD ω-2θ scan pattern of 10-period (a) BAlAs/GaAs and (b) BAlInAs/GaAs MQW samples grown at 610 °C.

BAlInAs alloy was uniform and GaAs/BAlInAs/GaAs sandwich structures could also be determined from the profiles. Unfortunately, the SIMS quantification of boron and indium could not be determined due to the lack of relative sensitivity factors (RSF).

3.3. BAlAs/GaAs and BAlInAs/GaAs MQW

Based on the research work mentioned above, 10-period $B_{0.019}Al_{0.981}As$/GaAs MQW and $B_{0.019}Al_{0.939}In_{0.042}As$/GaAs MQW structures had been grown on GaAs substrates, in which $B_{0.019}Al_{0.981}As$ or $B_{0.019}Al_{0.939}In_{0.042}As$ well thickness was 18 nm and GaAs barrier thickness was 45 nm. The DCXRD ω-2θ scan patterns are shown in Fig. 8, high-order satellite peaks of MQW structures could be clearly observed. However, compared with 10-period BGaAs/GaAs MQW and BGaInAs/GaAs MQW we had grown before [2], the number and the intensity of satellite peaks appearing in these DCXRD patterns decreased significantly, which is mainly due to the deterioration of the heterointerface abruptness caused by the larger surface roughness of BAlAs and BAlInAs layer.

4. Conclusion

In conclusion, we have demonstrated LP-MOCVD growth of zinc-blende $B_xAl_{1-x}As$ alloys with the boron composition x up to 2.8% on (0 0 1)GaAs substrates using TEB source. It has been found that boron incorporation into AlAs strongly depended on the susceptor coating, the growth temperature (T_g) and initial gas-phase boron mole fraction (X_v). The experimental results show that boron incorporation into AlAs could be enhanced significantly and the optimal growth temperature range of $B_xAl_{1-x}As$ alloys changed from 580 °C to 610 °C if SiC-coated graphite susceptors were replaced by the non-coated ones. Increasing X_v value at the constant T_g also led to the enhancement of boron incorporation into AlAs. However, the efficiency of incorporation boron into AlAs is still lower that that into GaAs. As boron composition x increased, RMS roughness of $B_xAl_{1-x}As$ samples increased sharply, BAs vibrational modes in the Raman spectra of $B_xAl_{1-x}As$ samples shifted to the higher energy side with a linear variation. By incorporating indium atoms into the BAlAs alloys, we have successfully deposited quaternary $B_xAl_{1-x-y}In_yAs$ alloys on GaAs substrates at 610 °C. DCXRD measurements show that $B_xAl_{1-x-y}In_yAs$ (x = 1.9%) alloy grown is lattice-matched to GaAs. In addition, 10-period BAlAs/GaAs and BAlInAs/GaAs MQW structures have also been successfully grown.

Acknowledgements

This work was supported by the National Basic Research Program of China (No. 2010CB327602), the National High Technology R&D Program of China (No. 2009AA03Z417), the National Natural Science Foundation of China (No. 61020106007), the Fundamental Research Funds for the Central Universities (BUPT2009RC0409) and the 111 Project (No. B07005).

References

[1] Q. Wang, X. Ren, F. Wang, J. Feng, J. Lv, J. Zhou, S. Cai, H. Huang, Y. Huang, Microelectron. J. 39 (2008) 1678–1682.
[2] Q. Wang, X. Ren, H. Huang, Y. Huang, S. Cai, Microelectron. J. 40 (2009) 87–91.
[3] R. Hamila, F. Saidi, P.H. Rodriguez, L. Auvray, Y. Monteil, H. Maaref, J. Alloys Compd. 506 (2010) 10–13.
[4] F. Saidi, R. Hamila, H. Maaref, Ph. Rodriguez, L. Auvray, Y. Monteil, J. Alloys Compd. 491 (2010) 45–48.
[5] J.F. Geisz, D.J. Friedman, S. Kurtz, J.M. Olson, A.B. Swartzlander, R.C. Reedy, A.G. Norman, J. Cryst. Growth 225 (2001) 372–376.
[6] J.F. Geisz, D.J. Friedman, J.M. Olson, S.R. Reedy, A.B. Swartzlander, B.M. Keyes, A.G. Norman, Appl. Phys. Lett. 76 (2000) 1143–1145.
[7] H. Patetzelt, V. Gottschalch, J. Bauer, G. Wagner, J. Cryst. Growth 298 (2007) 648–651.
[8] J.F. Geisz, D.J. Friedman, S. Kurtz, The Twenty-Eighth IEEE Photovoltaic Specialists Conference, 2000.
[9] G. Leibiger, C. Krahmer, J. Bauer, H. Herrnberger, V. Gottschalch, J. Cryst. Growth 272 (2004) 732–738.
[10] B. Kunert, S. Zinnkann, K. Volz, W. Stolz, J. Cryst. Growth 310 (2008) 4776–4779.
[11] H.M. Manasevit, W.B. Hewitt, A.J. Nelson, A.R. Mason, J. Electrochem. Soc. 136 (1989) 3070–3076.
[12] M.A. Tischler, P.M. Mooney, B.D. Parker, F. Cardone, M.S. Goorsky, J. Appl. Phys. 71 (1992) 984–992.
[13] V. Gottschalch, G. Leibiger, G. Benndorf, J. Cryst. Growth 248 (2003) 468–473.
[14] H. Dumont, J. Dazord, Y. Monteil, F. Alexandre, L. Goldstein, J. Cryst. Growth 248 (2003) 463–467.
[15] G. Leibiger, V. Gottschalch, V. Riede, M. Schubert, J.N. Hilfiker, T.E. Tiwald, Phys. Rev. B 67 (2003) 195205.